Available online at www.sciencedirect.com
ScienceDirect
Journal of Sound and Vibration 315 (2008) 816–835
JOURNAL OF SOUND AND VIBRATION
www.elsevier.com/locate/jsvi

Performance of vertically and obliquely reinforced 1–3 piezoelectric composites for active damping of laminated composite shells

M.C. Ray*, A.K. Pradhan

Department of Mechanical Engineering, Indian Institute of Technology, Kharagpur 721302, India

Received 16 May 2007; received in revised form 2 February 2008; accepted 10 February 2008
Handling Editor: L.G. Tham
Available online 8 April 2008

Abstract

This paper deals with the analysis of active constrained layer damping (ACLD) of laminated cylindrical composite shells using vertically and obliquely reinforced 1–3 piezoelectric composite materials as the material of the constraining layer of the ACLD treatment. A finite element model has been developed for analyzing the ACLD of laminated symmetric and antisymmetric cross-ply and angle-ply composite shells integrated with the patches of such ACLD treatment. Both in-plane and out-of-plane actuation of the constraining layer of the ACLD treatment has been utilized for deriving the finite element model. The analysis revealed that the vertical actuation dominates over the in-plane actuation. Particular emphasis has been placed on investigating the performance of the patches when the orientation angle of the piezoelectric fibers of the constraining layer is varied in the two mutually orthogonal vertical planes. The analysis revealed that the vertically reinforced 1–3 piezoelectric composites which are in general being used for the distributed sensors can be potentially used for the distributed actuators of high-performance light-weight smart cylindrical shells.

1. Introduction

Expediently, it was discovered that if the inherent properties of direct and converse piezoelectric effects present in the piezoelectric materials are exploited to use these materials as distributed sensors and actuators, respectively which are either mounted on or embedded in the flexible structures then the structures attain self-controlling and self-monitoring capabilities [1,2]. Such flexible structures having built-in mechanisms for self-controlling and self-monitoring capabilities are customarily known as ''Smart Structures''. Subsequently, extensive research has been carried out during the past several years [3–11] to demonstrate the use of piezoelectric materials for active control of vibration of high-performance light-weight smart structures. The piezoelectric coefficients of the existing monolithic piezoelectric materials are very small. Hence, the distributed actuators made of these monolithic piezoelectric materials need high-control voltage for satisfactory control of

*Corresponding author. Tel.: +91 3222 55221.
E-mail address: mcray@mech.iitkgp.ernet.in (M.C. Ray).

0022-460X/$ - see front matter © 2008 Elsevier Ltd. All rights reserved.
doi:10.1016/j.jsv.2008.02.012

vibrations of host structures. The research on the efficient use of these low-control-authority monolithic piezoelectric materials led to the development of active constrained layer damping (ACLD) treatment [12]. In ACLD treatment, the constraining layer is made of piezoelectric materials while the constrained layer is made of viscoelastic material. The control effort necessary for causing transverse shear deformations in the low stiff constrained viscoelastic layer of the ACLD treatment is compatible with the low-control authority of the existing monolithic piezoelectric materials. Hence, these piezoelectric materials perform much better to attenuate the vibration of smart structures when they are used for the constraining layer of the ACLD treatment than when they are directly bonded to the smart structures. Also, ACLD treatment provides the attributes of both passive and active damping occurring simultaneously because of the fact that passive damping mechanism is integral to this treatment [12,13]. Since its inception, extensive investigations have been performed to demonstrate the performance of ACLD treatment for active damping of plates [14,15], optimal control of plates [16] and shells [17].

Piezoelectric composite materials have now emerged as the new class of smart materials and find wide applications as distributed actuators and sensors of smart structures. In these new piezoelectric composite materials, the reinforcements are made of the existing monolithic piezoelectric materials and the matrix is the conventional epoxy. These piezoelectric composites provide wide range of effective material properties not offered by the existing monolithic piezoelectric materials, cause anisotropic actuation and are characterized by good conformability and strength integrity. Research on piezoelectric composite materials is mainly devoted to the micromechanical analysis for predicting their effective properties [18–28]. As a novel work, Arafa and Baz [29] investigated the performance of active damping piezoelectric composite for active control of an isotropic beam. In their work, the constrained viscoelastic layer of the ACLD treatment has been considered to be reinforced with piezoceramic fibers while the conventional isotropic layer has been used for the constraining layer of the treatment. Among the various piezoelectric composites proposed by the researchers till today, laminae of vertically reinforced 1–3 piezoelectric composites are commercially available [30] and are being effectively used for underwater transducers, medical imaging applications and high-frequency ultrasonic transducers [18,27]. The constructional feature of a lamina made of this 1–3 piezoelectric composite is that the piezoelectric fibers are vertically reinforced in the epoxy matrix along the thickness of the lamina while the fibers are poled vertically along their length. Since, in this lamina of 1–3 piezoelectric composite the fibers are vertically reinforced and the ends of the fibers are in contact with the surface electrodes, the applied voltage across these electrodes, i.e., across the thickness of the lamina creates the same electric fields in the thickness direction both in fibers and matrix. Thus the average electric field along the thickness direction of the homogenized lamina is equal to that in fibers and matrices. Also, since the magnitude of the piezoelectric coefficient e_{33} of the fiber material is much larger than that of the piezoelectric coefficient e_{31}, the magnitude of the effective piezoelectric coefficient e_{33} of vertically reinforced 1–3 piezoelectric composite material becomes larger than that of the effective coefficient e_{31} of this composite [18]. Therefore, if a voltage is applied across the surface electrodes of this lamina, the induced normal stress (σ_z) in the thickness direction will be larger than the induced in-plane normal stress (σ_x) and may be exploited for flexural vibration control. Hence, for these vertically reinforced 1–3 piezoelectric composites, the piezoelectric coefficient e_{33} is the key coefficient for electromechanical transduction. These composites are also characterized by improved mechanical performance, electromechanical coupling characteristics and acoustic impedance matching over the existing monolithic piezoelectric materials [18]. The other variations of constructional features of the commercially available 1–3 piezoelectric composites are that the piezoelectric fibers are obliquely reinforced in the matrix while they are coplanar with the vertical planes. However, very little attention has been paid to using these commercially available vertically and obliquely reinforced 1–3 piezoelectric composites as the material for distributed actuators of smart structures. Recently, Ray and Pradhan [31,32] examined the performance of these vertically/obliquely reinforced 1–3 piezoelectric composite for active damping of laminated composite beams and plates. They demonstrated that the vertical actuation by the 1–3 piezoelectric composite actuators causes significant improvement of damping characteristics of the laminated composite beams and plates. The laminated cylindrical shell is an important structural element and forms many critical structures. Also, the dynamical characteristics of laminated shells are different from that of plates. Thus a separate investigation is necessary for dynamic analysis of laminated shells. It seems that the performance of the vertically/obliquely reinforced 1–3 piezoelectric composites has not yet been studied for the purpose of active damping of laminated cylindrical composite shells.

In this paper, the authors intend to investigate the performance of vertically and obliquely reinforced 1–3 piezoelectric composites as the materials of the constraining layer of ACLD treatment for active damping of laminated cylindrical composite shells. For such investigation, three-dimensional analysis of ACLD of laminated cylindrical composite shells integrated with the patches of ACLD treatment has been carried out by the finite element method. The constraining layer of the ACLD treatment is considered to be made of vertically or obliquely reinforced 1–3 piezoelectric composite materials. The effect of piezoelectric fiber orientation in the two mutually orthogonal vertical planes on the performance of the patches of ACLD treatment has also been investigated.

2. Finite element modeling

Fig. 1 illustrates a clamped–free laminated composite shell composed of N number of orthotropic layers. The length, thickness and average radius of the shell are denoted by a, h and R, respectively. The top surface of the composite shell is integrated with the patches of ACLD treatment. The constraining layer of the patches of ACLD treatment is made of either vertically or obliquely reinforced 1–3 piezoelectric composite material. The constructional features of such 1–3 piezoelectric composite materials have been demonstrated in Fig. 2. For obliquely reinforced 1–3 piezoelectric composite, the piezoelectric fibers are coplanar with either the vertical xz or the yz plane making an angle ψ with the z-axis. The thickness of the piezoelectric composite layer and the viscoelastic layer are denoted by h_p and h_v, respectively. The middle plane of the substrate composite shell is considered as the reference plane. The origin of the curvilinear laminate coordinate system (xyz) is located on the reference plane such that the lines $x = 0$ and a indicate the ends of the shells. Denoted by k ($k = 1,2,3,\ldots,N+2$), the layer number of any layer of the overall shell, the thickness coordinates z of the top and bottom surface of any (kth) layer of the shell are represented by h_{k+1} and h_k, respectively. Also, the fiber orientation in any layer of the substrate shell in the plane (xy) of the lamina with respect to laminate coordinate system is denoted by θ.

The overall shell to be considered here is thin and consequently the first-order shear deformation theory (FSDT) can be used to model the axial displacements in all the layers of the overall shell. In Fig. 3, the kinematics of axial deformations of the overall shell based on the FSDT has been illustrated. Displayed in this figure, the variables u_0 and v_0 represent the generalized translational displacement of a point (x, y) on the reference plane ($z = 0$) along x and y directions, respectively; θ_x, ϕ_x and γ_x denote the generalized rotations of the normals to the middle planes of the substrate shell, the viscoelastic layer and the piezoelectric composite layer, respectively in the xz plane while θ_y, ϕ_y and γ_y represent their generalized rotations in the yz plane. According to the kinematics of deformations illustrated in Fig. 3, the axial displacements u and v at any point

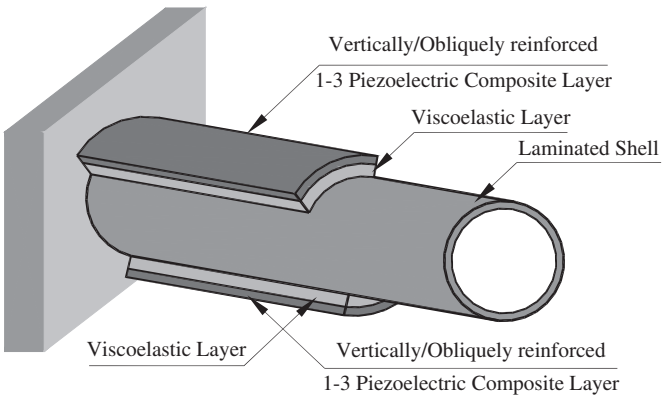

Fig. 1. Schematic representation of a laminated composite shell integrated with the patches of ACLD treatment composed of vertically/obliquely reinforced 1–3 piezoelectric composite constraining layer.

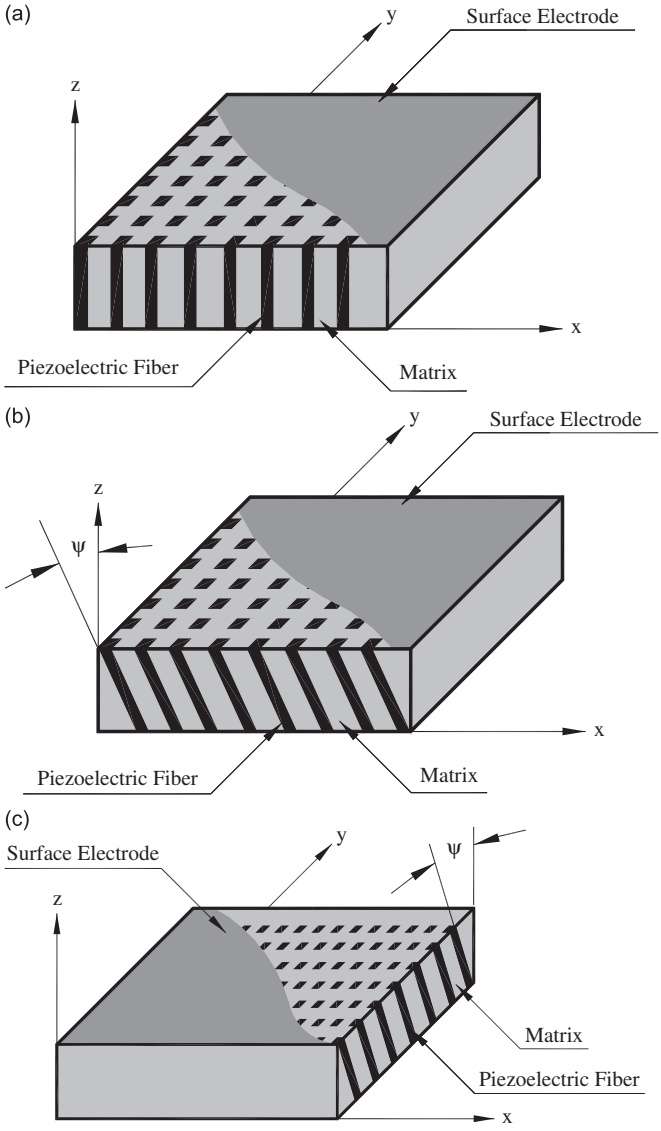

Fig. 2. Schematic diagrams of the laminae of vertically and obliquely reinforced 1–3 piezoelectric composites. (a) Lamina of vertically reinforced 1–3 piezoelectric composite, (b) piezoelectric fibers are coplanar with vertical xz plane and obliquely oriented, (c) piezoelectric fibers are coplanar with vertical yz plane and obliquely oriented.

in any layer of the overall shell along x and y directions, respectively, can be expressed as

$$u(x,y,z,t) = u_0(x,y,t) + (z - \langle z - h/2\rangle)\theta_x(x,y,t) + (\langle z - h/2\rangle - \langle z - h_{N+2}\rangle)\phi_x(x,y,t) + \langle z - h_{N+2}\rangle\gamma_x(x,y,t) \quad (1)$$

$$v(x,y,z,t) = v_0(x,y,t) + (z - \langle z - h/2\rangle)\theta_y(x,y,t) + (\langle z - h/2\rangle - \langle z - h_{N+2}\rangle)\phi_y(x,y,t) + \langle z - h_{N+2}\rangle\gamma_y(x,y,t) \quad (2)$$

in which, a function within the bracket $\langle\ \rangle$ represents the appropriate singularity functions.

Since the transverse actuation of the constraining layer of the ACLD treatment will be exploited for the control of vibration of the shells, the transverse normal strain in the overall shell must be considered in the model. Hence, for the sake of brevity, as the shell considered here is thin, the transverse displacement (w) at

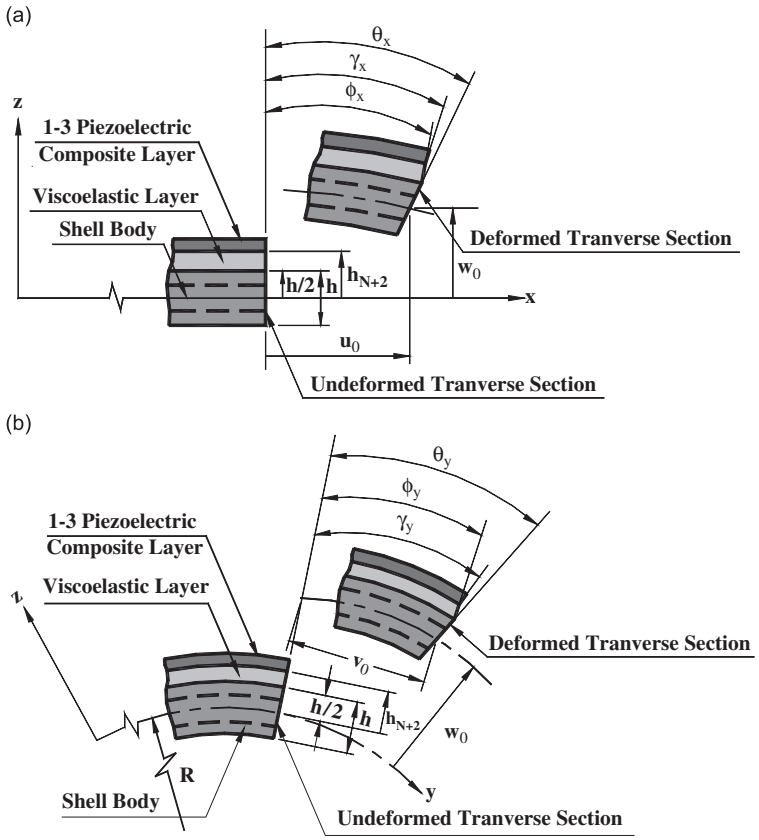

Fig. 3. (a) Deformation of any transverse cross-section of the laminated shell integrated with the ACLD treatment which is parallel to yz plane. (b) Deformation of any transverse cross-section of the laminated shell integrated with the ACLD treatment which is parallel to xz plane.

any point in the substrate shell, viscoelastic layer and the piezoelectric composite layer may be assumed to be linearly varying across their thicknesses. Thus the transverse displacement at any point in the overall shell is assumed as

$$w(x,y,z,t) = w_0(x,y,t) + (z - \langle z - h/2\rangle)\theta_z(x,y,t) + (\langle z - h/2\rangle - \langle z - h_{N+2}\rangle)\phi_z(x,y,t) + \langle z - h_{N+2}\rangle\gamma_z(x,y,t) \tag{3}$$

in which w_0 refers to the transverse displacement at any point on the reference plane; θ_z, ϕ_z and γ_z are the generalized displacements representing the gradients of the transverse displacement in the substrate shell, viscoelastic layer and the piezoelectric composite layer, respectively, with respect to the thickness coordinate (z).

For the ease of analysis, the generalized displacement variables are grouped into the two following vectors:

$$\{\mathbf{d}_t\} = [\,u_0 \quad v_0 \quad w_0\,]^{\mathrm{T}} \quad \text{and} \quad \{\mathbf{d}_r\} = [\,\theta_x \quad \theta_y \quad \theta_z \quad \phi_x \quad \phi_y \quad \phi_z \quad \gamma_x \quad \gamma_y \quad \gamma_z\,]^{\mathrm{T}} \tag{4}$$

In order to implement the selective integration rule for computing the element stiffness matrices corresponding to the transverse shear deformations, the state of strain at any point in the overall shell is divided into the following two strain vectors $\{\boldsymbol{\varepsilon}_b\}$ and $\{\boldsymbol{\varepsilon}_s\}$:

$$\{\boldsymbol{\varepsilon}_b\} = [\varepsilon_x \quad \varepsilon_y \quad \varepsilon_{xy} \quad \varepsilon_z]^{\mathrm{T}} \quad \text{and} \quad \{\boldsymbol{\varepsilon}_s\} = [\varepsilon_{xz} \quad \varepsilon_{yz}]^{\mathrm{T}} \tag{5}$$

in which $\varepsilon_x, \varepsilon_y, \varepsilon_z$ are the normal strains along x, y and z directions, respectively; ε_{xy} is the in-plane shear strain; and ε_{xz}, ε_{yz} are the transverse shear strains. By using the displacement fields (Eqs. (1)–(3)), the linear strain–displacement relations and Eq. (5), the vectors $\{\boldsymbol{\varepsilon}_b\}_c$, $\{\boldsymbol{\varepsilon}_b\}_v$ and $\{\boldsymbol{\varepsilon}_b\}_p$ defining the state of in-plane and

transverse normal strains at any point in the substrate composite shell, viscoelastic layer and the active constraining layer, respectively, can be expressed as

$$\{\boldsymbol{\varepsilon}_b\}_c = \{\varepsilon_{bt}\} + [\mathbf{Z}_1]\{\varepsilon_{br}\}, \quad \{\boldsymbol{\varepsilon}_b\}_v = \{\varepsilon_{bt}\} + [\mathbf{Z}_2]\{\varepsilon_{br}\} \quad \text{and} \quad \{\boldsymbol{\varepsilon}_b\}_p = \{\varepsilon_{bt}\} + [\mathbf{Z}_3]\{\boldsymbol{\varepsilon}_{br}\} \tag{6}$$

Similarly, the vectors $\{\in_s\}_c$, $\{\in_s\}_v$ and $\{\in_s\}_p$ defining the state of transverse shear strains at any point in the substrate composite shell, the viscoelastic layer and the active constraining layer, respectively, can be expressed as

$$\{\boldsymbol{\varepsilon}_s\}_c = \{\varepsilon_{st}\} + [\mathbf{Z}_4]\{\varepsilon_{sr}\}, \quad \{\boldsymbol{\varepsilon}_s\}_v = \{\varepsilon_{st}\} + [\mathbf{Z}_5]\{\varepsilon_{sr}\} \quad \text{and} \quad \{\boldsymbol{\varepsilon}_s\}_p = \{\varepsilon_{st}\} + [\mathbf{Z}_6]\{\varepsilon_{sr}\} \tag{7}$$

The various matrices appearing in Eqs. (6) and (7) have been defined in the Appendix while the generalized strain vectors are given by

$$\begin{aligned}
\{\boldsymbol{\varepsilon}_{bt}\} &= \left[\frac{\partial u_0}{\partial x} \quad \frac{\partial v_0}{\partial y} + \frac{w}{R} \quad \frac{\partial u_0}{\partial y} + \frac{\partial v_0}{\partial x} \quad 0\right]^{\mathrm{T}}, \ \{\boldsymbol{\varepsilon}_{st}\} = \left[\frac{\partial w_0}{\partial x} \quad \frac{\partial w_0}{\partial y} - \frac{v_0}{R}\right]^{\mathrm{T}}, \\
\{\boldsymbol{\varepsilon}_{br}\} &= \left[\frac{\partial \theta_x}{\partial x} \quad \frac{\partial \theta_y}{\partial y} \quad \frac{\partial \theta_x}{\partial y} + \frac{\partial \theta_y}{\partial x} \quad \theta_z \quad \frac{\partial \phi_x}{\partial x} \quad \frac{\partial \phi_x}{\partial x} \quad \frac{\partial \phi_x}{\partial y} + \frac{\partial \phi_y}{\partial x} \quad \phi_z \right. \\
&\quad \left. \frac{\partial \gamma_x}{\partial x} \quad \frac{\partial \gamma_y}{\partial y} \quad \frac{\partial \gamma_x}{\partial y} + \frac{\partial \gamma_y}{\partial x} \quad \gamma_z\right]^{\mathrm{T}} \quad \text{and} \\
\{\boldsymbol{\varepsilon}_{sr}\} &= \left[\theta_x \quad \theta_y \quad \phi_x \quad \phi_y \quad \gamma_x \quad \gamma_y \quad \frac{\partial \theta_z}{\partial x} \quad \frac{\partial \theta_z}{\partial y} \quad \frac{\partial \phi_z}{\partial x} \quad \frac{\partial \phi_z}{\partial y} \quad \frac{\partial \gamma_z}{\partial x} \quad \frac{\partial \gamma_z}{\partial y}\right]
\end{aligned} \tag{8}$$

Similar to the strain vectors given by Eq. (5), the state of stresses at any point in the overall shell are described by the following stress vectors:

$$\{\boldsymbol{\sigma}_b\} = [\,\sigma_x \quad \sigma_y \quad \sigma_{xy} \quad \sigma_z\,]^{\mathrm{T}} \quad \text{and} \quad \{\boldsymbol{\sigma}_s\} = [\,\sigma_{xz} \quad \sigma_{yx}\,]^{\mathrm{T}} \tag{9}$$

where σ_x, σ_y, σ_z are the normal stresses along x, y and z directions, respectively; σ_{xy} is the in-plane shear stresses; σ_{xz} and σ_{yz} are the transverse shear stresses.

The constitutive relations for the material of any orthotropic layer of the substrate shell are given by

$$\{\boldsymbol{\sigma}_b^k\} = [\mathbf{C}_b^k]\{\boldsymbol{\varepsilon}_b^k\} \quad \text{and} \quad \{\boldsymbol{\sigma}_s^k\} = [\mathbf{C}_s^k]\{\boldsymbol{\varepsilon}_s^k\}; \ (k = 1, 2, 3, \ldots, N) \tag{10}$$

where

$$[\mathbf{C}_b^k] = \begin{bmatrix} \bar{C}_{11}^k & \bar{C}_{12}^k & \bar{C}_{16}^k & \bar{C}_{13}^k \\ \bar{C}_{12}^k & \bar{C}_{22}^k & \bar{C}_{26}^k & \bar{C}_{23}^k \\ \bar{C}_{16}^k & \bar{C}_{26}^k & \bar{C}_{66}^k & \bar{C}_{36}^k \\ \bar{C}_{13}^k & \bar{C}_{23}^k & \bar{C}_{36}^k & \bar{C}_{33}^k \end{bmatrix}, \quad [\mathbf{C}_s^k] = \begin{bmatrix} \bar{C}_{55}^k & \bar{C}_{45}^k \\ \bar{C}_{45}^k & \bar{C}_{44}^k \end{bmatrix}$$

and $\bar{C}_{ij}^k$ $(i, j = 1,2,3,\ldots,6)$ are the transformed elastic coefficients with respect to the reference coordinate system. The material of the viscoelastic layer is assumed to be linearly viscoelastic and isotropic and is modeled by using the complex modulus approach. In the complex modulus approach, the shear modulus G and the Young's modulus E of the viscoelastic material are given by

$$G = G'(1 + i\eta) \quad \text{and} \quad E = 2G(1 + \upsilon) \tag{11}$$

in which G' is the storage modulus, υ is the Poisson's ratio and η is the loss factor at a particular operating temperature and frequency. Employing the complex modulus approach, the constitutive relations for the material of the viscoelastic layer $(k = N+1)$ can also be represented by Eq. (10) with $\bar{C}_{ij}^{N+1}$ $(i, j = 1,2,3,\ldots,6)$ being the complex elastic constants [13,14].

Following Smith and Auld [18], constitutive relations for the vertically reinforced $(\psi = 0^\circ)$ 1–3 piezocomposites are given by

$$\{\boldsymbol{\sigma}\} = [\mathbf{C}]_p\{\boldsymbol{\varepsilon}\} - [\mathbf{e}]\{\mathbf{E}\} \quad \text{and} \quad \{\mathbf{D}\} = [\mathbf{e}]^{\mathrm{T}}\{\boldsymbol{\varepsilon}\} + [\boldsymbol{\varepsilon}]\{\mathbf{E}\} \tag{12}$$

in which $[\mathbf{C}]_p$, $[\mathbf{e}]$ and $[\boldsymbol{\varepsilon}]$ are the effective elastic, piezoelectric and dielectric constant matrices, respectively. The explicit form of $[\mathbf{C}]_p$ resembles that of a specially orthotropic material while the explicit forms of $[\mathbf{e}]$ and $[\boldsymbol{\varepsilon}]$ are given by

$$[\mathbf{e}]^{\mathrm{T}} = \begin{bmatrix} 0 & 0 & 0 & 0 & e_{15} & 0 \\ 0 & 0 & 0 & e_{24} & 0 & 0 \\ e_{31} & e_{32} & e_{33} & 0 & 0 & 0 \end{bmatrix} \quad \text{and} \quad [\boldsymbol{\varepsilon}] = \begin{bmatrix} \varepsilon_{11} & 0 & 0 \\ 0 & \varepsilon_{22} & 0 \\ 0 & 0 & \varepsilon_{33} \end{bmatrix} \tag{13}$$

In Eq. (12), expressions for the stress $\{\boldsymbol{\sigma}\}$ and the strain $\{\boldsymbol{\varepsilon}\}$ vectors are not similar to those given in Eqs. (5) and (9), but are given by

$$\{\boldsymbol{\sigma}\} = [\sigma_x \quad \sigma_y \quad \sigma_z \quad \sigma_{yz} \quad \sigma_{xz} \quad \sigma_{xy}]^{\mathrm{T}} \quad \text{and} \quad \{\boldsymbol{\varepsilon}\} = [\varepsilon_x \quad \varepsilon_y \quad \varepsilon_z \quad \varepsilon_{yz} \quad \varepsilon_{xz} \quad \varepsilon_{xy}]^{\mathrm{T}} \tag{14}$$

while the electric field $\{\mathbf{E}\}$ and the electric displacement $\{\mathbf{D}\}$ vectors are given by

$$\{\mathbf{E}\} = [E_x \quad E_y \quad E_z]^{\mathrm{T}} \quad \text{and} \quad \{\mathbf{D}\} = [D_x \quad D_y \quad D_z]^{\mathrm{T}} \tag{15}$$

in which E_x, E_y and E_z are the electric fields along x, y and z directions, respectively and D_x, D_y and D_z are the corresponding electric displacements. When fibers of the 1–3 piezocomposite are coplanar with respect to the vertical xz- or yz-plane but their orientation angle with respect to the z-axis is ψ as shown in Fig. 2, the constitutive relations for such obliquely reinforced 1–3 piezocomposite with respect to the reference coordinate system (xyz) can be derived by employing the appropriate transformation law as follows:

$$\{\boldsymbol{\sigma}\} = [\bar{\mathbf{C}}]_p\{\varepsilon\}_p - [\bar{\mathbf{e}}]\{\mathbf{E}\} \quad \text{and} \quad \{\mathbf{D}\} = [\bar{\mathbf{e}}]^{\mathrm{T}}\{\boldsymbol{\varepsilon}\} + [\bar{\boldsymbol{\varepsilon}}]\{\mathbf{E}\} \tag{16}$$

where, $[\bar{\mathbf{C}}]_p = [\mathbf{T}]^{\mathrm{T}}[\mathbf{C}]_p[\mathbf{T}]$, $[\bar{\mathbf{e}}] = [\mathbf{T}]^{\mathrm{T}}[\mathbf{e}][\mathbf{R}]$ and $[\bar{\boldsymbol{\varepsilon}}] = [\mathbf{R}]^{-1}[\boldsymbol{\varepsilon}][\mathbf{R}]$. For fibers coplanar with the vertical xz plane as shown in Fig. 2, the transformation matrices $[\mathbf{T}]$ and $[\mathbf{R}]$ are given by

$$[\mathbf{T}]^{-1} = \begin{bmatrix} m^2 & 0 & n^2 & 0 & -mn & 0 \\ 0 & 1 & 0 & 0 & 0 & 0 \\ n^2 & 0 & m^2 & 0 & mn & 0 \\ 0 & 0 & 0 & m & 0 & n \\ 2mn & 0 & -2mn & 0 & m^2-n^2 & 0 \\ 0 & 0 & 0 & -n & 0 & m \end{bmatrix} \quad \text{and} \quad [\mathbf{R}] = \begin{bmatrix} m & 0 & n \\ 0 & 1 & 0 \\ -n & 0 & m \end{bmatrix} \tag{17}$$

while for fibers coplanar with the vertical yz plane these matrices are given by

$$[\mathbf{T}]^{-1} = \begin{bmatrix} 1 & 0 & 0 & 0 & 0 & 0 \\ 0 & m^2 & n^2 & -mn & 0 & 0 \\ 0 & n^2 & m^2 & mn & 0 & 0 \\ 0 & 2mn & -2mn & m^2-n^2 & 0 & 0 \\ 0 & 0 & 0 & 0 & m & -n \\ 0 & 0 & 0 & 0 & n & m \end{bmatrix} \quad \text{and} \quad [\mathbf{R}] = \begin{bmatrix} 1 & 0 & 0 \\ 0 & m & n \\ 0 & -n & m \end{bmatrix} \tag{18}$$

in which $m = \cos\psi$ and $n = \sin\psi$ In the present work, the applied electric field is considered only in the z direction and the stress and strain vectors are defined in a different manner as given by Eqs. (9) and (5). Hence, the constitutive equations given by Eq. (16) cannot be directly used in the present finite element formulation and are rearranged as follows:

$$\begin{aligned} &\{\boldsymbol{\sigma}_b^k\} = [\bar{\mathbf{C}}_b^k]\{\boldsymbol{\varepsilon}_b^k\} + [\bar{\mathbf{C}}_{bs}^k]\{\boldsymbol{\varepsilon}_s\} - \{\mathbf{e}_b\}\mathbf{E}_z, \quad \{\boldsymbol{\sigma}_s\} = [\bar{\mathbf{C}}_{bs}^k]^{\mathrm{T}}\{\boldsymbol{\varepsilon}_b\} + [\bar{\mathbf{C}}_s^k]\{\boldsymbol{\varepsilon}_s\} - \{\mathbf{e}_s\}\mathbf{E}_z, \quad \text{and} \\ &\mathbf{D}_z = \{\mathbf{e}_b\}^{\mathrm{T}}\{\boldsymbol{\varepsilon}_b^k\} + \{\mathbf{e}_s\}^{\mathrm{T}}\{\boldsymbol{\varepsilon}_s^k\} + \bar{\boldsymbol{\varepsilon}}_{33}\mathbf{E}_z, \quad k = N+2 \end{aligned} \tag{19}$$

It may be noted from Eqs. (19) that the transverse shear strains are coupled with the in-plane normal strains due to the orientation of piezoelectric fibers in the vertical xz- or yz-plane and the corresponding coupling

elastic constant matrices $[\bar{\mathbf{C}}_{bs}^{N+2}]$ are

$$[\bar{\mathbf{C}}_{bs}^{N+2}] = \begin{bmatrix} \bar{C}_{15} & \bar{C}_{25} & 0 & \bar{C}_{35} \\ 0 & 0 & \bar{C}_{46} & 0 \end{bmatrix} \quad \text{or} \quad [\bar{\mathbf{C}}_{bs}^{N+2}] = \begin{bmatrix} 0 & 0 & \bar{C}_{56} & 0 \\ \bar{C}_{14} & \bar{C}_{24} & 0 & \bar{C}_{34} \end{bmatrix} \tag{20}$$

as the piezoelectric fibers are coplanar with the vertical xz- or the vertical yz-plane, respectively. Note that if fibers are coplanar with both xz- and yz-planes (i.e. $\psi = 0^\circ$), this coupling matrix becomes a null matrix. Also, in the augmented form of constitutive relations (19) the transformed effective piezoelectric constant matrices $\{\mathbf{e}_b\}$ and $\{\mathbf{e}_s\}$ are given by

$$\{\mathbf{e}_b\} = [\,\bar{e}_{31} \quad \bar{e}_{32} \quad \bar{e}_{36} \quad \bar{e}_{33}\,]^{\mathrm{T}} \quad \text{and} \quad \{\mathbf{e}_s\} = [\,\bar{e}_{35} \quad \bar{e}_{34}\,]^{\mathrm{T}} \tag{21}$$

The principle of virtual work is employed to derive the governing equations of the overall shell/ACLD system and can be expressed as [14]

$$\sum_{k=1}^{N+2} \int_{\Omega} (\delta\{\boldsymbol{\varepsilon}_b^k\}^{\mathrm{T}}\{\boldsymbol{\sigma}_b^k\} + \delta\{\boldsymbol{\varepsilon}_s^k\}^{\mathrm{T}}\{\boldsymbol{\sigma}_s^k\} - \delta\mathbf{E}_z\bar{\varepsilon}_{33}\mathbf{E}_z - \delta\{\mathbf{d}_t\}^{\mathrm{T}}\rho^k\{\ddot{\mathbf{d}}_t\})\mathrm{d}\Omega - \int_A \delta\{\mathbf{d}_t\}^T\{f\}\mathrm{d}A = 0 \tag{22}$$

in which ρ^k is the mass density of the kth layer, $\{f\}$ is the externally applied surface traction acting over a surface area A and Ω represents the volume of the concerned layer. Since the shells under study are considered to be thin, the rotary inertia of the overall shell has been neglected in estimating the kinetic energy. The overall shell is discretized by eight-noded isoparametric quadrilateral elements. Following Eq. (9), the generalized displacement vectors, associated with the ith ($i = 1,2,3,\ldots,8$) node of the element can be written as

$$\{\mathbf{d}_{ti}\} = [\,u_{0i} \quad v_{0i} \quad w_{0i}\,]^{\mathrm{T}} \quad \text{and} \quad \{\mathbf{d}_{ri}\} = [\,\theta_{xi} \quad \theta_{yi} \quad \theta_{zi} \quad \phi_{xi} \quad \phi_{yi} \quad \phi_{zi} \quad \gamma_{xi} \quad \gamma_{yi} \quad \gamma_{zi}\,]^{\mathrm{T}} \tag{23}$$

Thus the generalized displacement vectors at any point within the element can be expressed in terms of the nodal generalized displacement vectors $\{\mathbf{d}_t^e\}$ and $\{\mathbf{d}_r^e\}$ as follows:

$$\{\mathbf{d}_t\} = [\mathbf{N}_t]\{\mathbf{d}_t^e\} \quad \text{and} \quad \{\mathbf{d}_r\} = [\mathbf{N}_r]\{\mathbf{d}_r^e\} \tag{24}$$

in which

$$\begin{aligned} &[\mathbf{N}_t] = [\,N_{t1} \quad N_{t2} \quad \cdots \quad N_{t8}\,]^{\mathrm{T}}, \quad [\mathbf{N}_r] = [\,N_{r1} \quad N_{r2} \quad \cdots \quad N_{r8}\,]^{\mathrm{T}}, \quad \mathbf{N}_{ti} = n_i\mathbf{I}_t, \quad \mathbf{N}_{ri} = n_i\mathbf{I}_r, \\ &\{\mathbf{d}_t^e\} = \left[\,\{d_{t1}^e\}^{\mathrm{T}} \quad \{d_{t2}^e\}^{\mathrm{T}} \quad \cdots \quad \{d_{t8}^e\}^{\mathrm{T}}\,\right]^{\mathrm{T}} \quad \text{and} \quad \{\mathbf{d}_r^e\} = \left[\,\{d_{r1}^e\}^{\mathrm{T}} \quad \{d_{r2}^e\}^{\mathrm{T}} \quad \cdots \quad \{d_{r8}^e\}^{\mathrm{T}}\,\right]^{\mathrm{T}} \end{aligned} \tag{25}$$

while $\mathbf{I}_t$ and $\mathbf{I}_r$ are the (3×3) and (9×9) identity matrices, respectively and n_i is the shape function of natural coordinates associated with the ith node. Making use of the relations given by Eqs. (6)–(8) and (24), the strain vectors at any point within the element can be expressed in terms of the nodal generalized displacement vectors as follows:

$$\begin{aligned} &\{\boldsymbol{\varepsilon}_b\}_c = [\mathbf{B}_{tb}]\{\mathbf{d}_t^e\} + [\mathbf{Z}_1][\mathbf{B}_{rb}]\{\mathbf{d}_r^e\}, \quad \{\boldsymbol{\varepsilon}_b\}_v = [\mathbf{B}_{tb}]\{\mathbf{d}_t^e\} + [\mathbf{Z}_2][\mathbf{B}_{rb}]\{\mathbf{d}_r^e\}, \\ &\{\boldsymbol{\varepsilon}_b\}_p = [\mathbf{B}_{tb}]\{\mathbf{d}_t^e\} + [\mathbf{Z}_3][\mathbf{B}_{rb}]\{\mathbf{d}_r^e\}, \quad \{\boldsymbol{\varepsilon}_s\}_c = [\mathbf{B}_{ts}]\{\mathbf{d}_t^e\} + [\mathbf{Z}_4][\mathbf{B}_{rs}]\{\mathbf{d}_r^e\}, \\ &\{\boldsymbol{\varepsilon}_s\}_v = [\mathbf{B}_{ts}]\{\mathbf{d}_t^e\} + [\mathbf{Z}_5][\mathbf{B}_{rs}]\{\mathbf{d}_r^e\} \quad \text{and} \quad \{\boldsymbol{\varepsilon}_s\}_p = [\mathbf{B}_{ts}]\{\mathbf{d}_t^e\} + [\mathbf{Z}_6][\mathbf{B}_{rs}]\{\mathbf{d}_r^e\} \end{aligned} \tag{26}$$

in which the nodal strain–displacement matrices $[\mathbf{B}_{tb}]$, $[\mathbf{B}_{rb}]$, $[\mathbf{B}_{ts}]$ and $[\mathbf{B}_{rs}]$ are given by

$$\begin{aligned} &[\mathbf{B}_{tb}] = [\,B_{tb1} \quad B_{tb2} \quad \cdots \quad B_{tb8}\,], \quad [\mathbf{B}_{rb}] = [\,B_{rb1} \quad B_{rb2} \quad \cdots \quad B_{rb8}\,], \\ &[\mathbf{B}_{ts}] = [\,B_{ts1} \quad B_{ts2} \quad \cdots \quad B_{ts8}\,] \quad \text{and} \quad [\mathbf{B}_{rs}] = [\,B_{rs1} \quad B_{rs2} \quad \cdots \quad B_{rs8}\,] \end{aligned} \tag{27}$$

The submatrices of $[\mathbf{B}_{tb}]$, $[\mathbf{B}_{rb}]$, $[\mathbf{B}_{ts}]$ and $[\mathbf{B}_{rs}]$ as shown in Eq. (27) have been explicitly presented in the Appendix. On substitution of Eqs. (20) and (26) into Eq. (22) and recognizing that $E_z = -V/h_p$ with V being the applied voltage across the thickness of the piezoelectric layer, one can derive the following open-loop

equations of motion of an element integrated with the ACLD treatment:

$$[\mathbf{M}^e]\{\ddot{\mathbf{d}}_t^e\} + [\mathbf{K}_{tt}^e]\{\mathbf{d}_t^e\} + [\mathbf{K}_{tr}^e]\{\mathbf{d}_r^e\} = \{\mathbf{F}_{tp}^e\}\mathbf{V} + \{\mathbf{F}^e\} \tag{28}$$

$$[\mathbf{K}_{rt}^e]\{\mathbf{d}_t^e\} + [\mathbf{K}_{rr}^e]\{\mathbf{d}_r^e\} = \{\mathbf{F}_{rp}^e\}\mathbf{V} \tag{29}$$

The elemental mass matrix ($[\mathbf{M}^e]$), the elemental stiffness matrices ($[\mathbf{K}_{tt}^e]$, $[\mathbf{K}_{tr}^e]$, $[\mathbf{K}_{rr}^e]$), the elemental electro-elastic coupling vectors ($\{\mathbf{F}_{tp}^e\}$, $\{\mathbf{F}_{rp}^e\}$), the elemental load vector $\{\mathbf{F}^e\}$ and the mass parameter ($\bar{m}$) appearing in Eqs. (28) and (29) are given by

$$\begin{aligned}
&[\mathbf{M}^e] = \int_0^{a_e}\int_0^{b_e} \bar{m}[\mathbf{N}_t]^{\mathrm{T}}[\mathbf{N}_t]\mathrm{d}x\,\mathrm{d}y, \quad [\mathbf{K}_{tt}^e] = [\mathbf{K}_{tb}^e] + [\mathbf{K}_{ts}^e] + [\mathbf{K}_{tbs}^e]_{pb} + [\mathbf{K}_{tbs}^e]_{ps},\\
&[\mathbf{K}_{tr}^e] = [\mathbf{K}_{trb}^e] + [\mathbf{K}_{trs}^e] + \tfrac{1}{2}([\mathbf{K}_{trbs}^e]_{pb} + [\mathbf{K}_{rtbs}^e]_{pb}^{\mathrm{T}} + [\mathbf{K}_{trbs}^e]_{ps} + [\mathbf{K}_{rtbs}^e]_{ps}^{\mathrm{T}}),\\
&[\mathbf{K}_{rt}^e] = [\mathbf{K}_{tr}^e]^{\mathrm{T}}, \quad [\mathbf{K}_{rr}^e] = [\mathbf{K}_{rrb}^e] + [\mathbf{K}_{rrs}^e] + [\mathbf{K}_{rrbs}^e]_{pb} + [\mathbf{K}_{rrbs}^e]_{ps}, \quad \{\mathbf{F}_{tp}^e\} = \{\mathbf{F}_{tb}^e\}_p + \{\mathbf{F}_{ts}^e\}_p,\\
&\{\mathbf{F}_{rp}^e\} = \{\mathbf{F}_{rb}^e\}_p + \{\mathbf{F}_{rs}^e\}_p, \quad \{\mathbf{F}^e\} = \int_0^{a_e}\int_0^{b_e} [\mathbf{N}_t]^{\mathrm{T}}\{f\}\,\mathrm{d}x\,\mathrm{d}y \quad \text{and} \quad \bar{m} = \sum_{k=1}^{N+2} \rho^k(h_{k+1} - h_k)
\end{aligned} \tag{30}$$

It should be noted from Eq. (30) that the elemental stiffness matrices associated with the transverse shear strains are derived separately such that the selective integration rule can be employed in a straight-forward manner to avoid the shear locking problem. The elemental stiffness matrices and the electro-elastic coupling vectors appearing in Eq. (30) corresponding to the bending-stretching deformations are

$$\begin{aligned}
&[\mathbf{K}_{tb}^e] = \int_A [\mathbf{B}_{tb}]^T([\mathbf{D}_{tb}] + [\mathbf{D}_{tb}]_v + [\mathbf{D}_{tb}]_p)[\mathbf{B}_{tb}]\mathrm{d}x\,\mathrm{d}y, \quad [\mathbf{K}_{tbs}^e]_{pb} = \int_A [\mathbf{B}_{tb}]^T[\mathbf{D}_{tbs}]_p[\mathbf{B}_{ts}]\mathrm{d}x\,\mathrm{d}y,\\
&[\mathbf{K}_{trb}^e] = \int_A [\mathbf{B}_{trb}]^T([\mathbf{D}_{trb}] + [\mathbf{D}_{trb}]_v + [\mathbf{D}_{trb}]_p)[\mathbf{B}_{rb}]\mathrm{d}x\,\mathrm{d}y,\\
&[\mathbf{K}_{trbs}^e]_{pb} = \int_A [\mathbf{B}_{tb}]^T[\mathbf{D}_{trbs}]_p[\mathbf{B}_{rs}]\mathrm{d}x\,\mathrm{d}y, \quad [\mathbf{K}_{rtbs}^e]_{pb} = \int_A [\mathbf{B}_{rb}]^T[\mathbf{D}_{rtbs}]_p[\mathbf{B}_{ts}]\mathrm{d}x\,\mathrm{d}y,\\
&[\mathbf{K}_{rrb}^e] = \int_A [\mathbf{B}_{rb}]^T([\mathbf{D}_{rrb}] + [\mathbf{D}_{rrb}]_v + [\mathbf{D}_{rrb}]_p)[\mathbf{B}_{rb}]\mathrm{d}x\,\mathrm{d}y, \quad [\mathbf{K}_{rrbs}^e]_{pb} = \int_A [\mathbf{B}_{rb}]^T[\mathbf{D}_{rrbs}]_p[\mathbf{B}_{rs}]\mathrm{d}x\,\mathrm{d}y,\\
&\{\mathbf{F}_{tb}^e\}_p = \int_A [\mathbf{B}_{tb}]^T\{\mathbf{D}_{tb}\}_p\mathrm{d}x\,\mathrm{d}y, \quad \{\mathbf{F}_{rb}^e\}_p = \int_A [\mathbf{B}_{rb}]^T\{\mathbf{D}_{rb}\}_p\mathrm{d}x\,\mathrm{d}y
\end{aligned} \tag{31}$$

and those associated with the transverse shear deformations are

$$\begin{aligned}
&[\mathbf{K}_{ts}^e] = \int_A [\mathbf{B}_{ts}]^{\mathrm{T}}([\mathbf{D}_{ts}] + [\mathbf{D}_{ts}]_v + [\mathbf{D}_{ts}]_p)[\mathbf{B}_{ts}]\mathrm{d}x\,\mathrm{d}y, \quad [\mathbf{K}_{tbs}^e]_{ps} = \int_A [\mathbf{B}_{ts}]^{\mathrm{T}}[\mathbf{D}_{tbs}]_p^{\mathrm{T}}[\mathbf{B}_{tb}]\mathrm{d}x\,\mathrm{d}y,\\
&[\mathbf{K}_{trs}^e] = \int_A [\mathbf{B}_{ts}]^{\mathrm{T}}([\mathbf{D}_{trs}] + [\mathbf{D}_{trs}]_v + [\mathbf{D}_{trs}]_p)[\mathbf{B}_{rs}]\mathrm{d}x\,\mathrm{d}y, \quad [\mathbf{K}_{trbs}^e]_{ps} = \int_A [\mathbf{B}_{ts}]^{\mathrm{T}}[\mathbf{D}_{rtbs}]_p^{\mathrm{T}}[\mathbf{B}_{rb}]\mathrm{d}x\,\mathrm{d}y,\\
&[\mathbf{K}_{rrs}^e] = \int_A [\mathbf{B}_{rs}]^{\mathrm{T}}([\mathbf{D}_{rrs}] + [\mathbf{D}_{rrs}]_v + [\mathbf{D}_{rrs}]_p)[\mathbf{B}_{rs}]\mathrm{d}x\,\mathrm{d}y, \quad [\mathbf{K}_{rtbs}^e]_{ps} = \int_A [\mathbf{B}_{rs}]^{\mathrm{T}}[\mathbf{D}_{trbs}]_p^{\mathrm{T}}[\mathbf{B}_{tb}]\mathrm{d}x\,\mathrm{d}y,\\
&[\mathbf{K}_{rrbs}^e]_{ps} = \int_A [\mathbf{B}_{rs}]^{\mathrm{T}}[\mathbf{D}_{rrbs}]_p^{\mathrm{T}}[\mathbf{B}_{rb}]\mathrm{d}x\,\mathrm{d}y, \quad \{\mathbf{F}_{ts}^e\}_p = \int_A [\mathbf{B}_{ts}]^{\mathrm{T}}\{\mathbf{D}_{ts}\}_p\mathrm{d}x\,\mathrm{d}y,\\
&\{\mathbf{F}_{rs}^e\}_p = \int_A [\mathbf{B}_{rs}]^{\mathrm{T}}\{\mathbf{D}_{rs}\}_p\mathrm{d}x\,\mathrm{d}y
\end{aligned} \tag{32}$$

The various rigidity matrices and the rigidity vectors for electro-elastic coupling appearing in the above elemental matrices are given by

$$[\mathbf{D}_{tb}]=\sum_{k=1}^{N}\int_{h_k}^{h_{k+1}}[\bar{\mathbf{C}}_b^k]\mathrm{d}z,\quad [\mathbf{D}_{trb}]=\sum_{k=1}^{N}\int_{h_k}^{h_{k+1}}[\mathbf{C}_b^k][\mathbf{Z}_1]\mathrm{d}z,\quad [\mathbf{D}_{rrb}]=\sum_{k=1}^{N}\int_{h_k}^{h_{k+1}}[\mathbf{Z}_1]^{\mathrm{T}}[\mathbf{C}_b^k][\mathbf{Z}_1]\mathrm{d}z,$$

$$[\mathbf{D}_{ts}]=\sum_{k=1}^{N}\int_{h_k}^{h_{k+1}}[\bar{\mathbf{C}}_s^k]\mathrm{d}z,\quad [\mathbf{D}_{trs}]=\sum_{k=1}^{N}\int_{h_k}^{h_{k+1}}[\mathbf{C}_b^k][\mathbf{Z}_4]\mathrm{d}z,\quad [\mathbf{D}_{rrs}]=\sum_{k=1}^{N}\int_{h_k}^{h_{k+1}}[\mathbf{Z}_4]^{\mathrm{T}}[\mathbf{C}_s^k][\mathbf{Z}_4]\mathrm{d}z,$$

$$[\mathbf{D}_{tb}]_v=h_v[\bar{\mathbf{C}}_b^{N+1}],\quad [\mathbf{D}_{trb}]_v=\int_{h_{N+1}}^{h_{N+2}}[\bar{\mathbf{C}}_b^{N+1}][\mathbf{Z}_2]\mathrm{d}z,\quad [\mathbf{D}_{rrb}]_v=\int_{h_{N+1}}^{h_{N+2}}[\mathbf{Z}_2]^{\mathrm{T}}[\bar{\mathbf{C}}_b^{N+1}][\mathbf{Z}_2]\mathrm{d}z,$$

$$[\mathbf{D}_{ts}]_v=h_v[\bar{\mathbf{C}}_s^{N+1}],\quad [\mathbf{D}_{trs}]_v=\int_{h_{N+1}}^{h_{N+2}}[\bar{\mathbf{C}}_s^{N+1}][\mathbf{Z}_5]\mathrm{d}z,\quad [\mathbf{D}_{rrs}]_v=\int_{h_{N+1}}^{h_{N+2}}[\mathbf{Z}_5]^{\mathrm{T}}[\bar{\mathbf{C}}_s^{N+1}][\mathbf{Z}_5]\mathrm{d}z,$$

$$[\mathbf{D}_{tb}]_p=h_p[\bar{\mathbf{C}}_b^{N+2}],\quad [\mathbf{D}_{trb}]_p=\int_{h_{N+2}}^{h_{N+3}}[\bar{\mathbf{C}}_b^{N+2}][\mathbf{Z}_3]\mathrm{d}z,\quad [\mathbf{D}_{rrb}]_p=\int_{h_{N+2}}^{h_{N+3}}[\mathbf{Z}_3]^{\mathrm{T}}[\bar{\mathbf{C}}_b^{N+2}][\mathbf{Z}_3]\mathrm{d}z,$$

$$[\mathbf{D}_{ts}]_p=h_p[\bar{\mathbf{C}}_s^{N+2}],\quad [\mathbf{D}_{trs}]_p=\int_{h_{N+2}}^{h_{N+3}}[\bar{\mathbf{C}}_s^{N+2}][\mathbf{Z}_6]\mathrm{d}z,\quad [\mathbf{D}_{rrs}]_p=\int_{h_{N+2}}^{h_{N+3}}[\mathbf{Z}_6]^{\mathrm{T}}[\bar{\mathbf{C}}_s^{N+2}][\mathbf{Z}_6]\mathrm{d}z,$$

$$[\mathbf{D}_{tbs}]_p=\int_{h_{N+2}}^{h_{N+3}}[\bar{\mathbf{C}}_{bs}^{N+2}]\mathrm{d}z,\quad [\mathbf{D}_{trbs}]_p=\int_{h_{N+2}}^{h_{N+3}}[\bar{\mathbf{C}}_{bs}^{N+2}][\mathbf{Z}_6]\mathrm{d}z,\quad [\mathbf{D}_{rtbs}]_p=\int_{h_{N+2}}^{h_{N+3}}[\mathbf{Z}_3]^{\mathrm{T}}[\bar{\mathbf{C}}_{bs}^{N+2}]\mathrm{d}z,$$

$$[\mathbf{D}_{rrbs}]_p=\int_{h_{N+2}}^{h_{N+3}}[\mathbf{Z}_3]^{\mathrm{T}}[\bar{\mathbf{C}}_{bs}^{N+2}][\mathbf{Z}_6]\mathrm{d}z,\quad \{\mathbf{D}_{tb}\}_p=\int_{h_{N+2}}^{h_{N+3}}-\{\bar{\mathbf{e}}_b\}/h_p\,\mathrm{d}z,$$

$$\{\mathbf{D}_{rb}\}_p=\int_{h_{N+2}}^{h_{N+3}}-[\mathbf{Z}_3]^{\mathrm{T}}\{\bar{\mathbf{e}}_b\}/h_p\,\mathrm{d}z,\quad \{\mathbf{D}_{ts}\}_p=\int_{h_{N+2}}^{h_{N+3}}-\{\bar{\mathbf{e}}_s\}/h_p\,\mathrm{d}z,\quad \{\mathbf{D}_{rs}\}_p=\int_{h_{N+2}}^{h_{N+3}}-[\mathbf{Z}_6]^{\mathrm{T}}\{\bar{\mathbf{e}}_s\}/h_p\,\mathrm{d}z \tag{33}$$

It may be noted now that since the elastic constant matrix of the viscoelastic layer is complex, the stiffness matrices of an element integrated with the ACLD treatment are complex. For an element without integrated with the ACLD treatment, the electro-elastic coupling matrices become null vectors and the elemental stiffness matrices will be real. It should also be noted that as the stiffness matrices associated with the transverse shear strains are derived separately, one can employ the selective integration rule to avoid the so-called shear locking problem in case of thin shells. Finally, the elemental equations of motion are assembled to obtain the open-loop global equation of motion of the overall shell integrated with the ACLD patches as follows:

$$[\mathbf{M}]\{\ddot{\mathbf{X}}\}+[\mathbf{K}_{tt}]\{\mathbf{X}\}+[\mathbf{K}_{tr}]\{\mathbf{X}_r\}=\sum_{j=1}^{q}\{\mathbf{F}_{tp}^j\}V^j+\{\mathbf{F}\} \tag{34}$$

and

$$[\mathbf{K}_{rt}]\{\mathbf{X}\}+[\mathbf{K}_{rr}]\{\mathbf{X}_r\}=\sum_{j=1}^{q}\{\mathbf{F}_{rp}^j\}V^j \tag{35}$$

where $[\mathbf{M}]$ is the global mass matrix, $[\mathbf{K}_{tt}]$, $[\mathbf{K}_{tr}]$ and $[\mathbf{K}_{rr}]$ are the global stiffness matrices, $\{\mathbf{F}_{tp}\}$, $\{\mathbf{F}_{rp}\}$ are the global electro-elastic coupling vectors, $\{\mathbf{X}\}$ and $\{\mathbf{X}_r\}$ are the global nodal generalized displacement vectors, $\{\mathbf{F}\}$ is the global nodal force vector, q is the number of patches and V^j is the voltage applied to the jth patch. Since the elemental stiffness matrices of an element augmented with the ACLD treatment are complex, the global stiffness matrices become complex and the energy dissipation characteristics of the overall shell are attributed to the imaginary part of these matrices. Hence, the global equations of motion as derived above also represent the passive (uncontrolled) constrained layer damping of the substrate shell when the constraining layer is not subjected to any control voltage following a derivative control law.

3. Closed-loop model

It is known that the ACLD treatment incorporates additional damping into the vibrating structures. This is accomplished by activating the constraining layer of each patch of the treatment with a control voltage proportional to the transverse velocity of a point. The location of this point for a specific patch will be defined in the next section. Thus the control voltage for each patch can be expressed in terms of the derivatives of the global nodal degrees of freedom as follows:

$$V^j = -k_d^j \dot{w} = -k_d^j [\mathbf{U}_t^j]\{\dot{\mathbf{X}}\} - k_d^j (h/2)[\mathbf{U}_r^j]\{\dot{\mathbf{X}}_r\} \tag{36}$$

where, k_d^j is the control gain for the jth patch, $[\mathbf{U}_t^j]$ and $[\mathbf{U}_r^j]$ are the unit vectors for expressing the transverse velocity of the point concerned in terms of the derivative of the global nodal generalized translational displacements. Substituting Eq. (36) into Eqs. (34) and (35), the final equations of motion governing the closed-loop dynamics of the overall shell/ACLD system can be obtained as follows:

$$[\mathbf{M}]\{\ddot{\mathbf{X}}\} + [\mathbf{K}_{tt}]\{\mathbf{X}\} + [\mathbf{K}_{tr}]\{\mathbf{X}_r\} + \sum_{j=1}^{m} k_d^j \{\mathbf{F}_{tp}^j\}[\mathbf{U}_t^j]\{\dot{\mathbf{X}}\} + \sum_{j=1}^{m} k_d^j (h/2)\{\mathbf{F}_{tp}^j\}[\mathbf{U}_r^j]\{\dot{\mathbf{X}}_r\} = \{\mathbf{F}\} \tag{37}$$

and

$$[\mathbf{K}_{rt}]\{\mathbf{X}\} + [\mathbf{K}_{rr}]\{\mathbf{X}_r\} + \sum_{j=1}^{m} k_d^j \{\mathbf{F}_{rp}^j\}[\mathbf{U}_t^j]\{\dot{\mathbf{X}}\} + \sum_{j=1}^{m} k_d^j (h/2)\{\mathbf{F}_{rp}^j\}[\mathbf{U}_r^j]\{\dot{\mathbf{X}}_r\} = 0 \tag{38}$$

4. Results and discussions

In this section, the numerical results obtained by the finite element model derived in the previous section have been presented. Symmetric as well as antisymmetric cross-ply and antisymmetric angle-ply thin cantilevered cylindrical shells integrated with two patches of ACLD treatment are considered as the numerical examples. The patches are placed 180° apart from each other on the outer surfaces of the shells and one of the ends of the patches is fixed at the clamped end of the shells. Note that the locations of the patches correspond to an optimal placement of ACLD treatments such that the controllability of the first two modes (1,2) and (1,1) becomes maximum [17]. The length of the patches is considered to be 66.67% of the length of the shells. Unless otherwise mentioned, the width of the patches is assumed to be one sixth of the outer circumference of the shells. PZT-5H/spur composite with 60% fiber volume fraction has been considered for the material of the constraining layer of the ACLD treatment. The elastic and piezoelectric properties of the vertically reinforced 1–3 piezoelectric composite layer with 60% fiber volume fraction are [32]

$$C_{11} = 9.29\,\text{GPa}, \quad C_{12} = 6.18\,\text{GPa}, \quad C_{13} = 6.05\,\text{GPa}, \quad C_{33} = 35.44\,\text{GPa}, \quad C_{23} = C_{13},$$
$$C_{44} = 1.58\,\text{GPa}, \quad C_{66} = 1.54\,\text{GPa}, \quad C_{55} = C_{44}, \quad e_{31} = -0.1902\,\text{C/m}^2, \quad e_{33} = 18.4107\,\text{C/m}^2$$

The transformation relations given by Eqs. (16)–(18) can be used to obtain the elastic and piezoelectric properties of the obliquely ($\psi \neq 0°$) reinforced 1–3 piezoelectric composite layer. The material properties considered for the orthotropic layers of the substrate shells are assumed as follows:

$$E_L = 172\,\text{GPa}, \quad E_L/E_T = 25, \quad G_{LT} = 0.5E_T, \quad v_{LT} = 0.25$$

in which the symbols have the usual meaning. The thicknesses of the constraining 1–3 piezoelectric composite layer, the viscoelastic layer and the laminated shells are considered to be 250 μm, 200 μm and 0.003 m, respectively, while the orthotropic layers of the substrate shells are of equal thickness. Also, the length and the value of R/h for the shells are considered as 1 m and 50, respectively. The complex shear modulus, Poisson's ratio and the density of the viscoelastic constrained layer are used as $20(1+i)\,\text{MN m}^{-2}$, 0.49 and $1140\,\text{kg m}^{-3}$, respectively [15].

In order to verify the validity of the present finite element model, the natural frequencies of the shells integrated with the inactivated patches of negligible thickness are first computed and subsequently compared

with the existing analytical results [33] of the identical shells without integrated with the patches. Table 1 demonstrates this comparison of the fundamental natural frequencies of certain shells. The nondimensional frequency parameter ϖ used for a particular shell has been considered according to the reference shown in Table 1 with which the present result for that shell is compared. It may be observed from this table that the results are in excellent agreement validating the model derived here.

The open-loop and closed-loop behavior of the shells are studied by the frequency response functions evaluated at a point (a, 0, $h/2$) on the top surface of the shells. A time-harmonic point force of magnitude 1 N is considered to act at the same point to excite the first few modes of the shells. The control voltage supplied to each patch is negatively proportional to the velocity of the point located on the outer shell surface that corresponds to the midpoint of the free width of the patch. The control gains are arbitrarily selected such that the first few modes are satisfactorily controlled while the value of control voltage is nominal. Figs. 4–6 illustrate the frequency response functions of clamped–cross-ply (0°/90°/0°), antisymmetric cross-ply (0°/90°/0°/90°) and antisymmetric angle-ply (−45°/45°/−45°/45°) shells, respectively when the fiber orientation angle (ψ) in the constraining layer is 0°. These figures display both uncontrolled and controlled responses and clearly reveal that the constraining layer made of vertically reinforced 1–3 piezoelectric composite material being studied here significantly attenuates the amplitude of vibrations, enhancing the damping characteristics of the laminated composite shells over the passive damping (uncontrolled). The maximum values of the control voltages required to compute the controlled responses presented in Figs. 4–6 have been found to be quite low and are illustrated in Fig. 7 for the symmetric cross-ply (0°/90°/0°) shell only. In order to investigate the contribution of vertical actuation in improving the damping characteristics of the shells as demonstrated in Figs. 4–6, active control responses of the symmetric cross-ply cantilever shell for a particular value of gain

Table 1
Comparison of fundamental natural frequency parameters ϖ of clamped–free shells

Shell type	R/h	a/R	Source	ϖ
0°/90°/0°	20	5	Present	0.4910
			Analytical [33]	0.4899
0°/90°	20	5	Present	0.5620
			Analytical [33]	0.5581

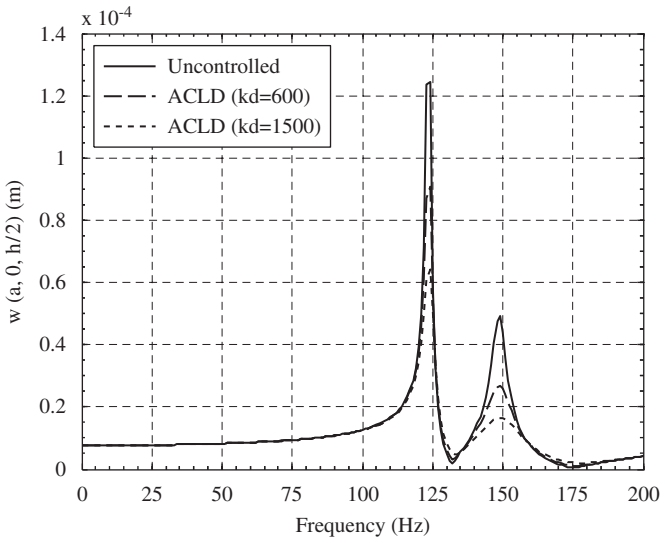

Fig. 4. Frequency response functions for the transverse displacement w (a, 0, $h/2$) of a cantilever symmetric cross-ply (0°/90°/0°) shell ($R/h = 50$, $\psi = 0°$).

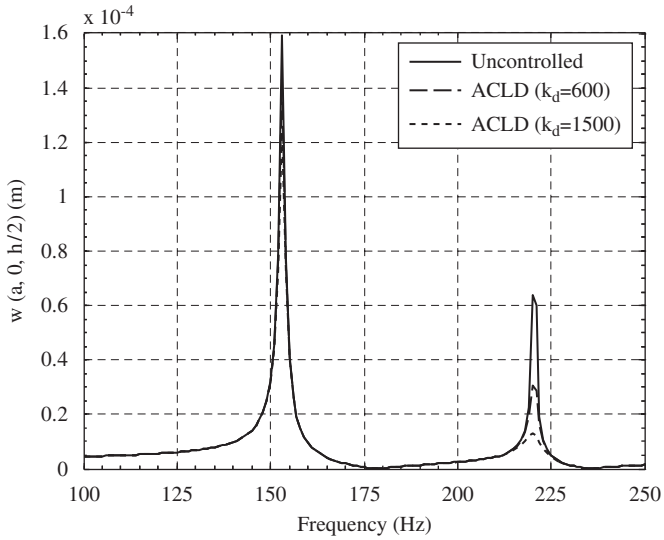

Fig. 5. Frequency response functions for the transverse displacement w (a, 0, $h/2$) of a cantilever antisymmetric cross-ply (0°/90°/0°/90°) shell ($R/h = 50$, $\psi = 0°$).

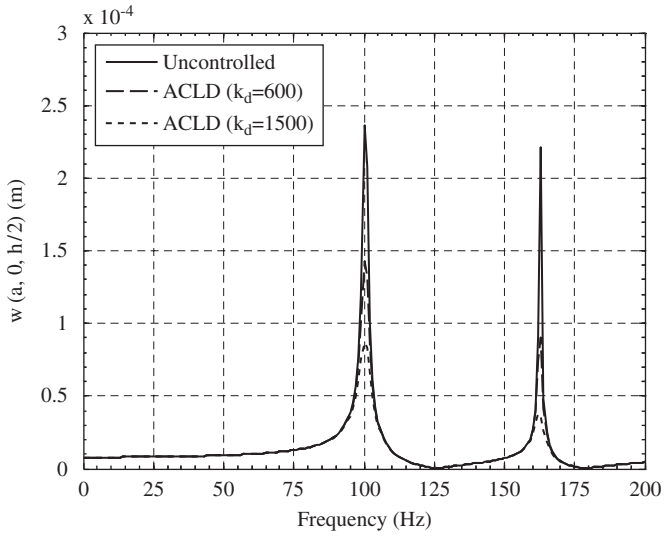

Fig. 6. Frequency response functions for the transverse displacement w (a, 0, $h/2$) of a cantilever antisymmetric angle-ply (−45°/45°/−45°/45°) shell ($R/h = 50$, $\psi = 0°$).

(1500) are plotted in Fig. 8 with and without considering the values of e_{33} and e_{31}. Note that when the value of e_{31} is zero and that of e_{33} is nonzero, the vertical actuation of the active constraining layer of the ACLD treatment is responsible for increasing the transverse shear deformation of the viscoelastic constrained layer over the passive counterpart resulting in improved damping of the smart shell over its passive damping. On the other hand, if e_{33} is zero and e_{31} is nonzero, the in-plane actuation of the active constraining layer causes increase in the transverse shear deformation of the viscoelastic core of the ACLD treatment leading to the improved overall damping of the smart shell. It is evident from Fig. 8 that the contribution of the piezoelectric coefficient e_{33} of the constraining vertically reinforced 1–3 piezoelectric composite layer on the attenuating capability of the ACLD treatment is significantly larger than that of the piezoelectric coefficient e_{31} of the constraining layer for controlling the modes displayed in Fig. 8. Although not shown here, similar results are

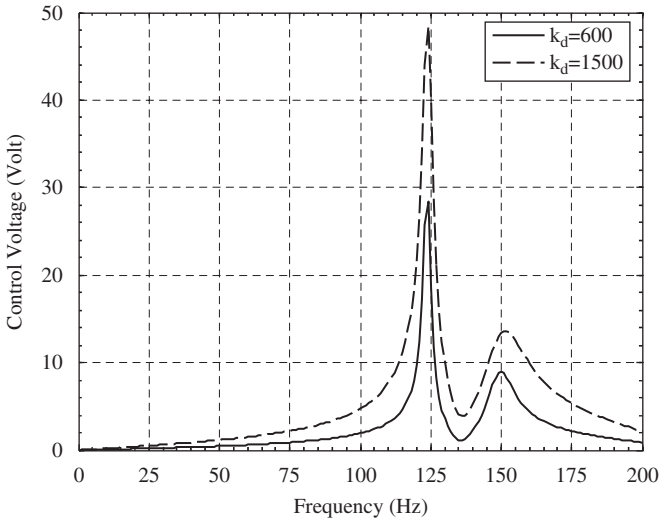

Fig. 7. Control voltage for the active damping of the cantilever symmetric cross-ply (0°/90°/0°) shell shown in Fig. 4.

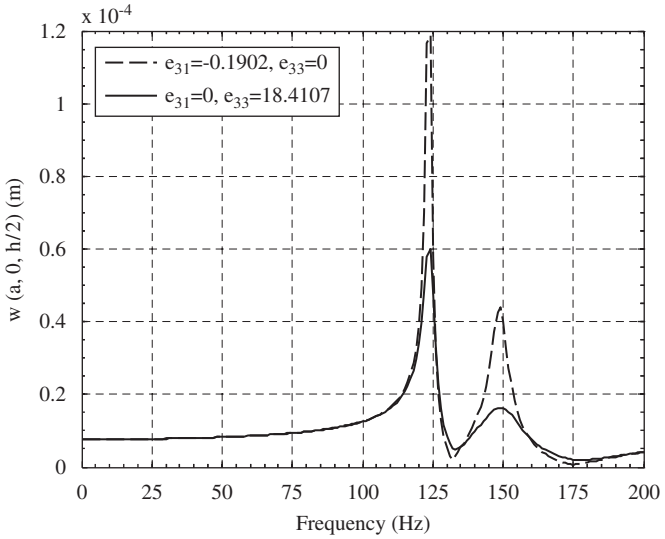

Fig. 8. Frequency response functions demonstrating the contribution of e_{33} on the controlled responses for the transverse displacement w (a, 0, $h/2$) of the cantilever symmetric cross-ply (0°/90°/0°) shell (gain = 1500, $R/h = 50$, $\psi = 0°$).

also obtained for antisymmetric cross-ply and angle-ply shells. Since the piezoelectric coefficient e_{33} of the 1–3 piezoelectric composite constraining layer has major contribution in improving the active damping of smart shells as manifested by Fig. 8, one must consider the transverse normal strain of the constraining layer of the ACLD treatment even if it is made of monolithic piezoelectric materials with $|e_{33}| > |e_{31}|$ for accurate theoretical analysis of active damping of smart structures.

The effect of variation of piezoelectric fiber angle in the vertical xz and yz planes on the performance of the patches has been studied. The maximum value of fiber orientation angle (ψ) in the commercially available obliquely reinforced 1–3 piezoelectric composite is 45° [30]. Hence, for studying the effect of piezoelectric fiber orientation on the performance of the patches, the orientation angle (ψ) of the fibers is varied from 0° to 45°. In this regard, it should be noted that for investigating the effect of variation of piezoelectric fiber angle (ψ) in the constraining layer of the patches on the performance of the patches, the value of ψ has been smoothly

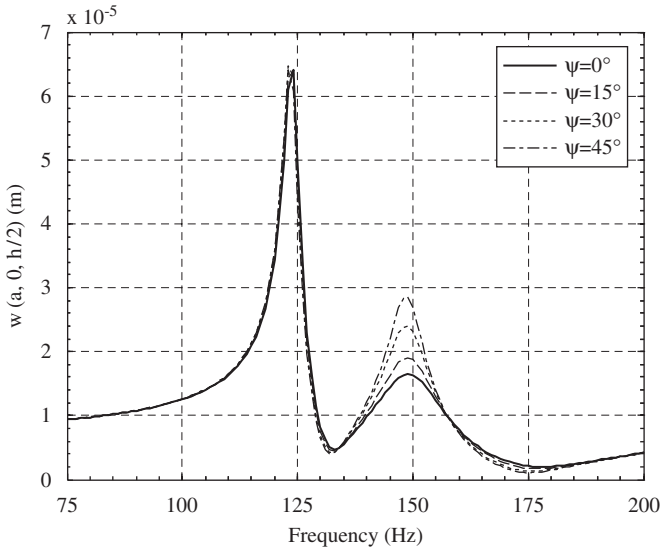

Fig. 9. Effect of variation of fiber orientation (ψ) on the performance of the patches for controlling a cantilever symmetric cross-ply (0°/90°/0°) shell when the piezoelectric fibers of the constraining layer are coplanar with the xz plane (gain = 1200, $R/h = 50$).

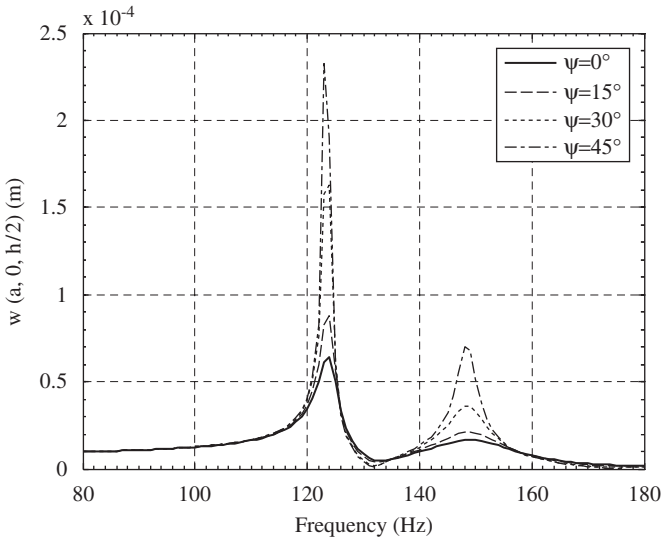

Fig. 10. Effect of variation of fiber orientation (ψ) on the performance of the patches for controlling a cantilever symmetric cross-ply (0°/90°/0°) shell when the piezoelectric fibers of the constraining layer are coplanar with the yz plane (gain = 1500, $R/h = 50$).

varied to compute the controlled responses. However, for the sake of clarity in the plots, the responses corresponding to the four specific values of ψ have been presented such that the optimum performance of the patches can be demonstrated. Figs. 9 and 10 demonstrate the effect of piezoelectric fiber orientation on the performance of the patches for improving the damping characteristics of cantilever symmetric cross-ply substrate shells when the orientation of the piezoelectric fibers is varied in the vertical xz and yz plane, respectively. These figures illustrate that the attenuating capability of the patches becomes maximum when the orientation angle (ψ) of the fibers in xz and yz plane is 0°. Fig. 11 demonstrates the effect of variation of piezoelectric fiber orientation angle (ψ) in the xz plane on the performance of the patches for improving the damping characteristics of a four-layered cantilever antisymmetric cross-ply substrate shell. It may be

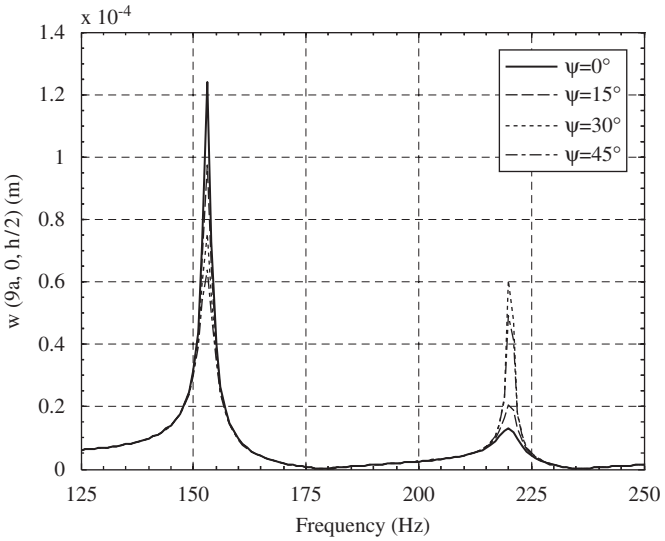

Fig. 11. Effect of variation of fiber orientation (ψ) on the performance of the patches for controlling a cantilever antisymmetric cross-ply ($0^\circ/90^\circ/0^\circ/90^\circ$) shell when the piezoelectric fibers of the constraining layer are coplanar with the xz plane (gain = 1500, $R/h = 50$).

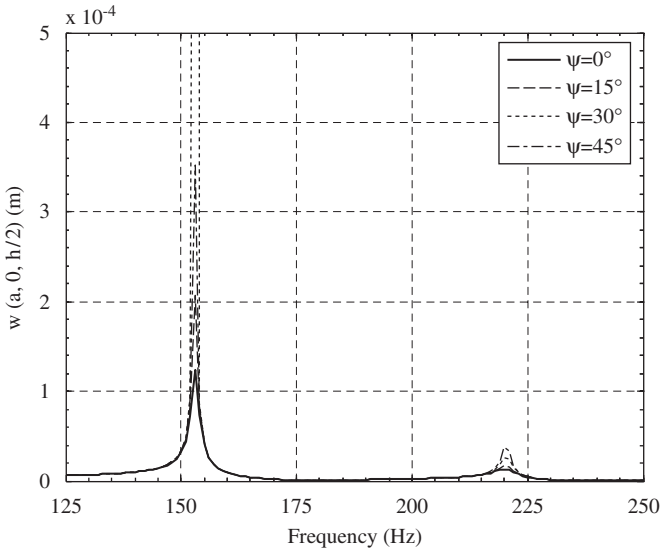

Fig. 12. Effect of variation of fiber orientation (ψ) on the performance of the patches for controlling a cantilever antisymmetric cross-ply ($0^\circ/90^\circ/0^\circ/90^\circ$) shell when the piezoelectric fibers of the constraining layer are coplanar with the yz plane (gain = 1200, $R/h = 50$).

observed from this figure that the attenuating capability of the patches becomes maximum for controlling the first and second modes if the fiber orientation angle (ψ) is 45° and 0°, respectively. When the fiber orientation is varied in yz plane, the attenuating capability of the patches for controlling these modes becomes maximum when the fiber orientation angle (ψ) is 0° as shown in Fig. 12. For a four-layered antisymmetric angle-ply shell, Figs. 13 and 14 demonstrate the effect of variation of piezoelectric fiber orientation in xz and yz planes, respectively, on the performance of the patches for improving the damping characteristics of a four-layered cantilever antisymmetric angle-ply ($-45^\circ/45^\circ/-45^\circ/45^\circ$) substrate shell. It may be observed from these figures that the controllability of the patches for controlling both modes of the shell becomes maximum when the orientation angle (ψ) of the fibers in xz plane is 45°.

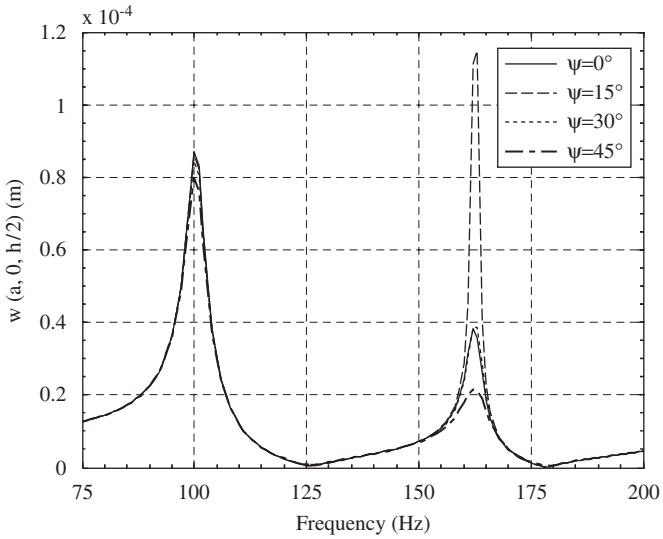

Fig. 13. Effect of variation of fiber orientation (ψ) on the performance of the patches for controlling a cantilever antisymmetric cross-ply ($-45°/45°/-45°/45°$) shell when the piezoelectric fibers of the constraining layer are coplanar with the xz plane (gain = 1500, $R/h = 50$).

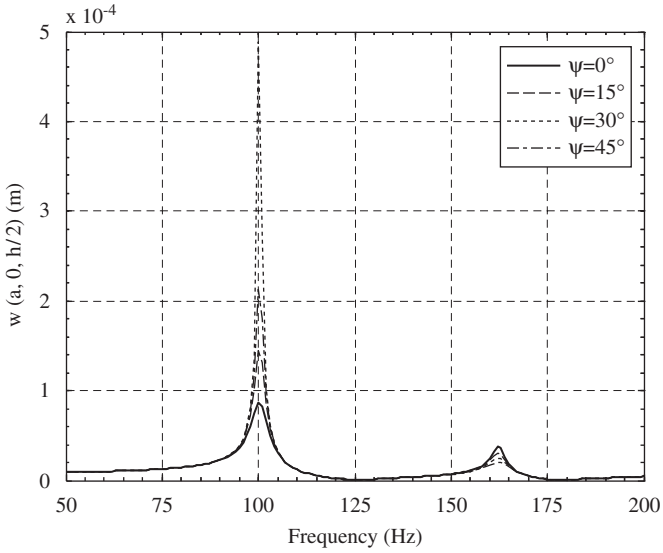

Fig. 14. Effect of variation of fiber orientation (ψ) on the performance of the patches for controlling a cantilever antisymmetric cross-ply ($-45°/45°/-45°/45°$) shell when the piezoelectric fibers of the constraining layer are coplanar with the yz plane (gain = 1400, $R/h = 50$).

5. Conclusions

In this paper, a study has been carried out to investigate the performance of vertically and obliquely reinforced 1–3 piezoelectric composite materials as the material for distributed actuator of smart laminated composite shells. A finite element model has been developed to describe the dynamics of the shells integrated with the patches of ACLD treatment and the constraining layer of the ACLD treatment is considered to be composed of the vertically reinforced 1–3 piezoelectric composite material. Unlike the existing finite element models of smart structures integrated with ACLD treatment, the derivation of the present finite element model includes the transverse deformation of the substrate shells, the constrained viscoelastic layer and the

constraining 1–3 piezoelectric composite layer of the ACLD treatment along the thickness (i.e. z) direction such that both vertical and in-plane actuations of the constraining layer of the patches can be utilized for active damping of the shells. The finite element model is based on FSDT. Symmetric/antisymmetric cross-ply and antisymmetric angle-ply laminated cantilever shells are considered for evaluation of numerical results. Two patches of ACLD treatment are used which are optimally placed on the outer surface of the shells such that the first two modes are efficiently controlled. The frequency responses of the symmetric cross-ply, antisymmetric cross-ply and angle-ply composite shells indicate that the active constraining layer of the ACLD treatment made of vertically reinforced piezoelectric composite material significantly enhances the damping characteristics of the shells over the passive damping. The analysis revealed that if the vertically reinforced 1–3 piezoelectric composite material is used for the constraining layer of ACLD treatment, then the contribution of vertical actuation of the constraining layer alone for improving the active damping characteristics of the smart composite shells is significantly larger than that due to the in-plane actuation of the constraining layer alone. The fundamental differences between the existing analyses of ACLD and the present analysis are that both in-plane and vertical actuations of the constraining layer of the present ACLD treatment have been utilized in the present model for improving the active damping and vertical actuation dominates over the in-plane actuation while the existing analyses are only concerned with the utilization of in-plane actuation of the constraining layer. It is important to note from the present investigation that the variation of orientation angle of the piezoelectric fibers of the constraining layer in the vertical xz and yz planes of the shells affects the performance of the patches. The performance of the patches becomes maximum for controlling the symmetric cross-ply shells when the orientation angle (ψ) of the fibers in xz and yz planes is 0°. To attain the best performance of the patches for controlling the first mode of antisymmetric cross-ply shells, the piezoelectric fibers of the constraining layer should be oriented in xz plane and the orientation angle (ψ) should be 45° while for controlling the second mode the orientation angle should be 0°. If the constraining layer of the patches is made of obliquely reinforced 1–3 piezoelectric composite and the orientation angle of the piezoelectric fibers is 45° in xz plane, then the performance of the patches becomes maximum for controlling the four-layered antisymmetric angle-ply $(-45^\circ/45^\circ/-45^\circ/45^\circ)$ shell.

Appendix

In Eqs. (6) and (7), the matrices $[\mathbf{Z}_1]$, $[\mathbf{Z}_2]$, $[\mathbf{Z}_3]$, $[\mathbf{Z}_4]$, $[\mathbf{Z}_5]$ and $[\mathbf{Z}_6]$ are given by

$$[\mathbf{Z}_1] = [\,[\bar{\mathbf{Z}}_1] \quad \tilde{\mathbf{o}} \quad \tilde{\mathbf{o}}\,], \quad [\mathbf{Z}_2] = [\,(h/2)\mathbf{I} \quad [\bar{\mathbf{Z}}_2] \quad \tilde{\mathbf{o}}\,], \quad [\mathbf{Z}_3] = [\,(h/2)\mathbf{I} \quad h_v\mathbf{I} \quad [\bar{\mathbf{Z}}_3]\,],$$

$$[\mathbf{Z}_4] = [\,[\bar{\mathbf{Z}}_4] \quad \bar{\mathbf{o}} \quad \bar{\mathbf{o}} \quad z\bar{\mathbf{I}} \quad \bar{\mathbf{o}} \quad \bar{\mathbf{o}}\,], \quad [\mathbf{Z}_5] = \left[\frac{h}{2R}\mathbf{I}_1 \quad [\bar{\mathbf{Z}}_5] \quad \bar{\mathbf{o}} \quad (h/2)\bar{\mathbf{I}} \quad (z-h/2)\bar{\mathbf{I}} \quad \bar{\mathbf{o}}\right],$$

$$[\mathbf{Z}_6] = \left[\frac{h}{2R}\mathbf{I}_1 \quad \frac{h_v}{R}\mathbf{I}_1 \quad \bar{Z}_6 \quad (h/2)\bar{\mathbf{I}} \quad h_v\bar{\mathbf{I}} \quad (z-h_{N+2})\bar{\mathbf{I}}\right]$$

in which

$$[\bar{\mathbf{Z}}_1] = \begin{bmatrix} z & 0 & 0 & 0 \\ 0 & z & 0 & \dfrac{z}{R} \\ 0 & 0 & z & 0 \\ 0 & 0 & 0 & 1 \end{bmatrix}, \quad [\bar{\mathbf{Z}}_2] = \begin{bmatrix} (z-h/2) & 0 & 0 & 0 \\ 0 & (z-h/2) & 0 & \dfrac{(z-h/2)}{R} \\ 0 & 0 & (z-h/2) & 0 \\ 0 & 0 & 0 & 1 \end{bmatrix},$$

$$[\bar{\mathbf{Z}}_3] = \begin{bmatrix} (z-h_{N+2}) & 0 & 0 & 0 \\ 0 & (z-h_{N+2}) & 0 & (z-h_{N+2})/R \\ 0 & 0 & (z-h_{N+2}) & 0 \\ 0 & 0 & 0 & 1 \end{bmatrix},$$

$$[\bar{\mathbf{Z}}_4]=\begin{bmatrix}1 & 0\\ 0 & \dfrac{z}{R}\end{bmatrix},\quad [\bar{\mathbf{Z}}_5]=\begin{bmatrix}1 & 0\\ 0 & 1-(z-h/2)/R\end{bmatrix},\quad [\bar{\mathbf{Z}}_6]=\begin{bmatrix}1 & 0\\ 0 & 1-(z-h_{N+2})/R\end{bmatrix},$$

$$\mathbf{I}=\begin{bmatrix}1 & 0 & 0 & 0\\ 0 & 1 & 0 & \dfrac{1}{R}\\ 0 & 0 & 1 & 0\\ 0 & 0 & 0 & 0\end{bmatrix},\quad \mathbf{I}_1=\begin{bmatrix}0 & 0\\ 0 & -1\end{bmatrix},\quad \bar{\mathbf{I}}=\begin{bmatrix}1 & 0\\ 0 & 1\end{bmatrix},\quad \bar{\mathbf{o}}=\begin{bmatrix}0 & 0\\ 0 & 0\end{bmatrix}\quad \text{and}\quad \tilde{\mathbf{o}}=\begin{bmatrix}\bar{o} & \bar{o}\\ \bar{o} & \bar{o}\end{bmatrix}$$

The various submatrices $\mathbf{B}_{tbi}$, $\mathbf{B}_{tsi}$, $\mathbf{B}_{rbi}$ and $\mathbf{B}_{rsi}$ appearing in Eq. (27) are given by

$$\mathbf{B}_{tbi}=\begin{bmatrix}\dfrac{\partial n_i}{\partial x} & 0 & 0\\ 0 & \dfrac{\partial n_i}{\partial y} & 1/R\\ \dfrac{\partial n_i}{\partial y} & \dfrac{\partial n_i}{\partial x} & 0\\ 0 & 0 & 0\end{bmatrix},\quad \mathbf{B}_{tsi}=\begin{bmatrix}0 & 0 & \dfrac{\partial n_i}{\partial x}\\ 0 & -1/R & \dfrac{\partial n_i}{\partial y}\end{bmatrix},\quad \mathbf{B}_{rbi}=\begin{bmatrix}\bar{\mathbf{B}}_{rbi} & \widehat{0} & \widehat{0}\\ \widehat{0} & \bar{\mathbf{B}}_{rbi} & \widehat{0}\\ \widehat{0} & \widehat{0} & \bar{\mathbf{B}}_{rbi}\end{bmatrix},$$

$$\bar{\mathbf{B}}_{rbi}=\begin{bmatrix}\dfrac{\partial n_i}{\partial x} & 0 & 0\\ 0 & \dfrac{\partial n_i}{\partial y} & 0\\ \dfrac{\partial n_i}{\partial y} & \dfrac{\partial n_i}{\partial x} & 0\\ 0 & 0 & 1\end{bmatrix},\quad \mathbf{B}_{rsi}=\begin{bmatrix}\widehat{\mathbf{I}} & \breve{0} & \breve{0}\\ \breve{0} & \widehat{\mathbf{I}} & \breve{0}\\ \breve{0} & \breve{0} & \widehat{\mathbf{I}}\\ \bar{\mathbf{B}}_{rsi} & \breve{0} & \breve{0}\\ \breve{0} & \bar{\mathbf{B}}_{rsi} & \breve{0}\\ \breve{0} & \breve{0} & \bar{\mathbf{B}}_{rsi}\end{bmatrix},\quad \bar{\mathbf{B}}_{rsi}=\begin{bmatrix}0 & 0 & \dfrac{\partial n_i}{\partial x}\\ 0 & 0 & \dfrac{\partial n_i}{\partial y}\end{bmatrix}\quad \text{and}$$

$$\widehat{\mathbf{I}}=\begin{bmatrix}1 & 0 & 0\\ 0 & 1 & 0\end{bmatrix}$$

where in $\widehat{0}$, and $\breve{0}$ are the (4×3) and (2×3) null matrices, respectively.

References

[1] T. Bailey, J.E. Hubbard, Distributed piezoelectric polymer active vibration control of a cantilever beam, *Journal of Guidance, Control and Dynamics* 8 (5) (1985) 605–611.

[2] E.F. Crawley, J.D. Luis, Use of piezoelectric actuators as elements of intelligent structures, *AIAA Journal* 25 (10) (1987) 1373–1385.

[3] A. Baz, S. Poh, Performance of an active control system with piezoelectric actuators, *Journal of Sound and Vibration* 126 (2) (1988) 327–343.

[4] C.K. Lee, W.W. Chiang, O. Sulivan, Piezoelectric modal sensor/actuator pairs for critical active damping vibration control, *Journal of the Acoustical Society of America* 90 (1) (1991) 374–384.

[5] S. Hanagud, M.W. Obal, A.J. Calise, Optimal vibration control by the use of piezoceramic sensors and actuators, *Journal of Guidance, Control and Dynamics* 15 (5) (1992) 1199–1206.

[6] Y. Gu, R.L. Clark, C.R. Fuller, Experiments on active control of plate vibration using piezoelectric actuators and polyvinylidyne fluoride (PVDF) modal sensors, *ASME Journal of Vibrations and Acoustics* 116 (1994) 303–308.

[7] A. Baz, S. Poh, Optimal vibration control with modal positive position feedback, *Optimal Control Applications and Methods* 17 (1996) 141–149.

[8] B.N. Agarwal, K.E. Treanor, Shape control of a beam using piezoelectric actuators, *Smart Materials and Structures* 8 (1999) 729–740.

[9] S. Dong, L. Tong, Vibration control of plates using discretely distributed piezoelectric quasi-modal actuators/sensors, *AIAA Journal* 39 (2001) 1766–1772.

[10] M.C. Ray, Optimal control of laminated shells with piezoelectric sensor and actuator layers, *AIAA Journal* 41 (6) (2003) 1151–1157.

[11] F. Peng, Alfred Ng, Yan-Ru Hu, Actuator placement optimization and adaptive vibration control of plate smart structures, *Journal of Intelligent Material Systems and Structures* 16 (2005) 263–271.
[12] B. Azvine, G.R. Tomlinson, R.J. Wynne, Use of active constrained layer damping for controlling resonant, *Smart Materials and Structures* 4 (1995) 1–6.
[13] M.C. Ray, A. Baz, Optimization of energy dissipation of active constrained layer damping treatments of plates, *Journal of Sound and Vibration* 208 (1997) 391–406.
[14] Y.S. Jeung, I.Y. Shen, Development of isoparametric, degenerate constrained layer element for plate and shell structures, *AIAA Journal* 39 (10) (2001) 1997–2005.
[15] C. Chantalakhana, R. Stanway, Active constrained layer damping of clamped–clamped plate vibrations, *Journal of Sound and Vibration* 241 (5) (2001) 755–777.
[16] J. Ro, A. Baz, Optimum placement and control of active constrained layer damping using modal strain energy approach, *Journal of Vibration and Control* 8 (2002) 861–876.
[17] M.C. Ray, J.N. Reddy, Optimal control of thin circular cylindrical shells using active constrained layer damping treatment, *Smart Materials and Structures* 13 (1) (2004) 64–72.
[18] W.A. Smith, B.A. Auld, Modeling 1–3 composite piezoelectrics: thickness mode oscillations, *IEEE Transactions on Ultrasonics, Ferroelectrics and Frequency Control* 31 (1) (1991) 40–47.
[19] Y. Benveniste, G.J. Dvorak, Uniform fields and universal relations in piezoelectric composites, *Journal of the Mechanics and Physics of Solids* 40 (6) (1992) 1295–1312.
[20] M.L. Dunn, M. Taya, Micromechanics predictions of the effective electroelastic modulli of piezoelectric composites, *International Journal of Solids and Structures* 30 (1993) 161–175.
[21] J. Bennet, G. Hayward, Design of 1–3 piezoelectric composite hydrophones using finite element analysis, *IEEE Transactions on Ultrasonics, Ferroelectrics and Frequency Control* 44 (1997) 565–574.
[22] J. Aboudi, Micromechanical prediction of the effective coefficients of thermo-piezoelectric multiphase composites, *Journal of Intelligent Material Systems and Structures* 9 (1998) 713–722.
[23] O. Sigmund, S. Torquato, I.A. Aksay, On the design of 1–3 piezocomposite using topology optimization, *Journal of Material Research* 13 (1998) 1038–1048.
[24] Jian Guo Wan, B.Q. Tao, Design and study on a 1–3 anisotropy piezocomposite sensor, *Materials and Design* 21 (2000) 533–576.
[25] X. Ruan, T.W. Chou, A 3-D connectivity model for effective piezoelectric properties of yarn composites, *Journal of Composite Materials* 36 (14) (2002) 1693–1708.
[26] P. Tan, L. Tong, A microelectromechanics model for 3-D PFRC materials, *Journal of Composite Materials* 36 (2) (2002) 127–141.
[27] L.C. Hellen, Li Kun, L.C. Chung, Piezoelectric ceramic fiber/epoxy 1–3 composite for high frequency ultrasonic transducer application, *Materials Science and Engineering B* 99 (2003) 29–35.
[28] N. Mallik, M.C. Ray, Effective coefficients of piezoelectric fiber-reinforced composites, *AIAA Journal* 41 (4) (2003) 704–710.
[29] M. Arafa, A. Baz, Dynamics of active piezoelectric damping composites, *Composites: Part B* 31 (2000) 255–264.
[30] Piezocomposites, Materials Systems Inc., 543 Great Road, Littleton, MA 01460.
[31] M.C. Ray, A.K. Pradhan, Performance of vertically reinforced 1–3 piezoelectric composites for active damping of smart structures, *Smart Materials and Structures* 15 (1) (2006) 631–641.
[32] M.C. Ray, A.K. Pradhan, On the use of vertically reinforced 1–3 piezoelectric composites for hybrid damping of laminated composite plates, *Mechanics of Advanced Materials and Structures* 14 (4) (2007) 245–261.
[33] Messina, K.P. Soldatos, Ritz-type dynamic analysis of cross-ply laminated circular cylinders subjected to different boundary conditions, *Journal of Sound and Vibration* 227 (1999) 749–768.